ELSEVIER

Contents lists available at ScienceDirect

## **Materials Today Physics**

journal homepage: www.journals.elsevier.com/materials-today-physics





# Defect diamond-like tellurides as infrared nonlinear optical materials with giant second-harmonic generation tensor

Mengran Sun<sup>a,b</sup>, Chunxiao Li<sup>a,b</sup>, Jinlong Shi<sup>a,b</sup>, Ming-Hsien Lee<sup>c,\*\*</sup>, Jiyong Yao<sup>a,b,\*</sup>

- <sup>a</sup> Beijing Center for Crystal Research and Development, Key Lab of Functional Crystals and Laser Technology, Technical Institute of Physics and Chemistry, Chinese Academy of Sciences, Beijing, 100190, PR China
- b Center of Materials Science and Optoelectronics Engineering, University of Chinese Academy of Sciences, Beijing, 100049, PR China
- <sup>c</sup> Department of Physics, Tamkang University, Tamsui, New Tapei, 25137, Taiwan

#### ARTICLE INFO

Keywords:
Defect diamond-like
Infrared nonlinear optical
Tellurides
Second-harmonic generation
First-principles calculation

### ABSTRACT

As promising candidate for mid- and far-infrared (MFIR) nonlinear optical (NLO) materials, diamond-like (DL) chalcogenides have been extensively studied because of their considerable advantages. Among them, tellurides attract our attention as their stronger electron polarization and wider transmittance range than those of sulfides and selenides. Herein, the insightful structural characteristics and NLO properties of defect DL MGa<sub>2</sub>Te<sub>4</sub> (M = Zn, Cd) were studied for the first time at experimental and theoretical level. They crystallize in the noncentrosymmetric I-4 space group (No.82), with a three-dimensional structure consisting of highly oriented [MTe<sub>4</sub>] and [GaTe<sub>4</sub>] tetrahedra, which can be viewed as derived from AgGaS<sub>2</sub> (AGS). Experimental results illustrate that MGa<sub>2</sub>Te<sub>4</sub> (M = Zn, Cd) exhibits moderate band gaps, strong SHG intensities about 4.9–10.6 times that of AGSe at 90-125 µm, and congruent-melting behavior. Theoretical calculations based on E-field DFPT method indicate that the tremendous SHG tensors  $d_{14}$  of  $ZnGa_2Te_4$  and  $CdGa_2Te_4$  are 127.67 and 105.19 pm/V. SHG-density analysis reveals that the lone-pair packets of Te ions in [GaTe<sub>4</sub>] units are the main source of SHG responses. In addition, calculations on Mulliken bond order index imply that the main difference between these two crystals is the bonding modes of M-Te. Special care was also given to ensure convergence of k-mesh for both conventional and primitive cells of the crystals, with two different methods for calculating linear and non-linear optical properties compared side by side. This work demonstrates the potential applications of these two defect DL tellurides in the MFIR NLO field.

### 1. Introduction

Over the years, second-order nonlinear optical (NLO) materials have received continuous attention and are facing increasing demands in optoelectronic and photonic frontiers [1–5]. Among them, mid- and far-infrared (MFIR) nonlinear optical crystals are indispensable components of IR solid-state lasers, which can be widely applied in military and civil fields, such as laser sensing, communications, environmental monitoring, minimally invasive medical surgery, etc. [6–12] Currently, commercial MFIR NLO materials mainly include AgGaS<sub>2</sub> (AGS), AgGaSe<sub>2</sub> (AGSe), and ZnGeP<sub>2</sub> (ZGP) [13–15]. On the one hand, their higher power laser outputs are seriously impeded due to their intrinsic defects. On the other hand, AGS and ZGP exhibit strong multi-phonon

absorption near 9  $\mu$ m, and cannot cover the "8–14  $\mu$ m" atmospheric transparent window [16–18]. Therefore, searching for new IR NLO materials with longer IR cutoff edges is of great interest.

Metal chalcogenides have long been regarded as potential candidates for IR NLO materials because of their diverse structures and relatively large second-harmonic-generation (SHG) effect, especially those with diamond-like (DL) structural features [19–24]. Inspiringly, many IR NLO optical materials with DL structure have been reported under unremitting efforts, including LiGaQ2 (Q = S, Se) [25], LiInS2 [26], Li2CdM^IVS4 (M^IV = Ge, Sn) [27], Li2MnM^IVS4 (M^IV = Ge, Sn) [28,29], Li2ZnM^IVSe4 (M^IV = Ge, Sn) [30,31], Cu2M^IISnS4 (M^II = Zn, Cd) [32,33], Li4MgGe2S7 [34]. In the DL structures, if the cation sites are not fully occupied, these structures are named defect DL structures [35].

E-mail addresses: mhslee@mail.tku.edu.tw (M.-H. Lee), jyao@mail.ipc.ac.cn (J. Yao).

<sup>\*</sup> Corresponding author. Beijing Center for Crystal Research and Development, Key Lab of Functional Crystals and Laser Technology, Technical Institute of Physics and Chemistry, Chinese Academy of Sciences, Beijing, 100190, PR China.

<sup>\*\*</sup> Corresponding author.

Correspondingly, the valence electrons concentration (VEC) changes due to the existence of cation vacancies, which provides an opportunity to optimize optical performance. Taking HgGa<sub>2</sub>S<sub>4</sub> as an example, which VEC number is 4.57. The existence of vacancies modulates the comprehensive properties of HgGa<sub>2</sub>S<sub>4</sub> (Eg = 2.84 eV,  $3 \times AGS$ ) [36]. Another ternary defect DL compound, InPS<sub>4</sub>, whose larger VEC number (VEC = 5.33) implies that it has less cation sites than HgGa<sub>2</sub>S<sub>4</sub> does. InPS<sub>4</sub> also exhibits a wide band gap of 3.12 eV and a large SHG coefficient of about 25 pm/V [37]. Furthermore, several defect-DL compounds have been successfully synthesized and proved to be potential IR NLO materials, including Hg<sub>3</sub>P<sub>2</sub>S<sub>8</sub> (Eg = 2.82 eV; 3.6 × AGS) [38], MgGa<sub>2</sub>Se<sub>4</sub> (Eg = 2.96 eV;  $d_{14}$  = -20.07 pm/V) [39], LiZnPS<sub>4</sub> (Eg = 3.76 eV;  $d_{36}$  = 10.42 pm/V) [40], AgZnPS<sub>4</sub> (Eg = 3.21 eV;  $d_{36}$  = 26.66 pm/V) [41], AgHgPS<sub>4</sub> (Eg = 2.63 eV; 5.09 × AGS) [41], and CuZnPS<sub>4</sub> (Eg = 3.0 eV;  $d_{14}$  = 15.9 pm/V) [23].

Among metal chalcogenides, metal tellurides are promising MFIR NLO crystal candidates due to their relatively large electron polarization and wider IR transparency range than those of sulfides and selenides [42–44]. Taking AGQ2 (Q = S, Se, Te) as an example, AgGaTe2 exhibits larger SHG coefficient, broader IR transparency range, but with a small band gap ( $d_{\rm eff}=77$  pm/V,  $\sim\!21$  µm,  $E_g=1.316$  eV), compared to AGS (13.4 pm/V,  $\sim\!11$  µm,  $E_g=2.58$  eV) and AGSe (36 pm/V,  $\sim\!17$  µm,  $E_g=1.83$  eV) [45]. In order to optimize the comprehensive properties of tellurides, the introduction of transition metals such as  $Zn^{2+}$  and  $Cd^{2+}$  into the structures might have certain advantages for increasing the band gap [18,46]. On the one hand, these elements avoid the d-d or f-f optical transitions, and on the other hand, they hardly occupy the top of the valence band (VB) and the bottom of the conduction band (CB), which are beneficial to the enlargement of the band gap.

Based on the above discussions, we conducted in-depth research on the database of inorganic crystal structures, and discovered the transition metal tellurides  $MGa_2Te_4$  (M=Zn, Cd) with defect DL structure. These compounds were first reported by Hahn et al., in 1955 [47]. Then, Fouad et al. and Kumar et al. synthesized  $MGa_2Te_4$  thin films and illustrated that they are good solar photovoltaic material [48,49]. Furthermore, Prakash et al. and Liu et al. indicated that  $MGa_2Te_4$  system can serve as potential thermoelectric materials [50,51]. However, a comprehensive study of their IR NLO properties and structural features has been overlooked. This work is driven by their potential defect

diamond-like structure, and the SHG performance is evaluated from the aspects of experiment and theoretical calculation, which makes up for the blank of previous studies. Since these compounds contain two NLO active structural components, namely [Zn/CdTe<sub>4</sub>] and [GaTe<sub>4</sub>] tetrahedra. The synergistic interaction between the above-mentioned chromophores may be beneficial to generate a good balance between a strong SHG response and a large optical band gap. In this work, MGa<sub>2</sub>Te<sub>4</sub> (M = Zn, Cd) were independently synthesized by heating the binary raw materials, and the linear and nonlinear optical properties of title compounds were systematically investigated by experiments and First-principles calculations.

### 2. Results and discussion

### 2.1. Crystal structures

The isostructural compounds MGa<sub>2</sub>Te<sub>4</sub> (M = Zn, Cd) are uniaxial defect DL compounds and crystallize in the non-centrosymmetric I-4 (No.82) space group. The asymmetric unit consists of one crystallographically independent Zn/Cd atom (Wyckoff position: 2a), two Ga atoms (Ga1: 2b; Ga2: 2c), and one Te atom (8g). These compounds feature a three-dimensional (3D) framework. As illustrated in Fig. 1, taking ZnGa<sub>2</sub>Te<sub>4</sub> as an example, the Zn atom is tetrahedral coordinated to the Te atoms with Zn-Te bond length of 2.673 (7) Å and the Te-Zn-Te angles range from 106.327 to 111.066°, implying negligible distortion of the [ZnTe<sub>4</sub>] tetrahedra. Similarly, the Ga atoms also bonded with four Te atoms to form [GaTe<sub>4</sub>] tetrahedra with Ga-Te distance of 2.612 (7) Å and the Te-Ga-Te angles range from 104.307 to 112.113° in [Ga1Te<sub>4</sub>] unit, while Ga-Te bond length in [Ga2Te<sub>4</sub>] tetrahedra is 2.638 (7) Å, and the Te-Ga-Te angles range from 105.176 to 118.452° (Fig. 1e). Then, one [ZnTe<sub>4</sub>] and two [GaTe<sub>4</sub>] tetrahedra are interconnected by sharing corner Te atoms to form [ZnGa2Te4] cluster, which are further aligned along the bc plane via corner-sharing to constitute the 2 o [ZnGa2Te4] layer (Fig. 1c). These layers are stacked along a axis and linked by shared corner Te atoms to build a 3D framework (Fig. 1a and b). Notably, the defect DL structure of ZnGa<sub>2</sub>Te<sub>4</sub> can be seen as evolved from the normal DL structure of AgGaS<sub>2</sub>, as depicted in Fig. 1d. Half of the Ag <sup>+</sup> cations are replaced by divalent Zn<sup>2+</sup>, and the remaining half of the metal sites are vacancy defects, which makes the VEC number of ZnGa<sub>2</sub>Te<sub>4</sub> equal to

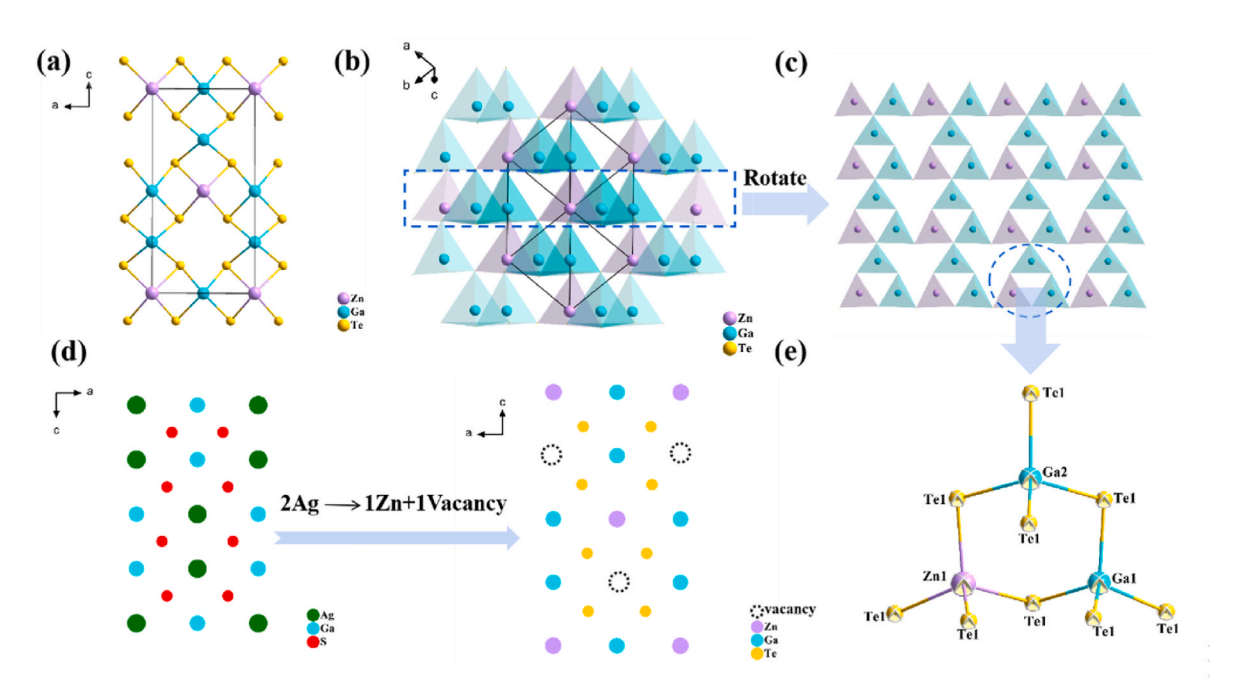


Fig. 1. Crystal structure of  $ZnGa_2Te_4$ . (a) the unit cell of  $ZnGa_2Te_4$  viewed along b axis; (b) the 3D framework of  $ZnGa_2Te_4$  composed of corner-sharing [ $ZnTe_4$ ] and [ $ZnTe_4$ ] tetrahedra; (c) the  $Z_{\infty}$ [ $ZnGa_2Te_4$ ] layer; structure evolution from AGS to  $ZnGa_2Te_4$  (d); (e) thermal vibration ellipsoid of the asymmetric unit.

4.57. Excitingly,  $ZnGa_2Te_4$  inherits the parallel arrangement of all NLO-active groups in the AGS structure, which facilitates the efficient superposition of the microscopic second-order nonlinear susceptibility. Compared with the tetrahedral coordination of the S atom in AGS, the Te ions in  $ZnGa_2Te_4$  only connects with three cations due to the presence of vacancies (Fig. S1), resulting in the occurrence of non-bonded electrons.

#### 2.2. Purity and composition

The phase purity of the MGa<sub>2</sub>Te<sub>4</sub> (M = Zn, Cd) powder was accessed by using Rietveld refinement. As shown in Fig. 2a and 2b, the observed X-ray diffraction patterns are in good agreement with the calculated ones, indicating the purity of MGa<sub>2</sub>Te<sub>4</sub> polycrystalline powder. In addition, results of Rietveld refinement for ZnGa2Te4 and CdGa2Te4 with fixed atomic parameters were given in Table S1. The parameters characterizing the goodness of fit (R-values and  $\chi^2$ ) also support the purity of the experimental powder. The bond lengths and angles of MGa<sub>2</sub>Te<sub>4</sub> (M = Zn, Cd) obtained by Rietveld refinement are also summarized in Tables S2 and S4. The unit cell parameters, bond lengths, and angles of title compounds obtained by Rietveld refinement are in good agreement with the previously reported results, which proves the structural features of title compounds (Tables S3 and S5). SEM images in Fig. 2c and 2d clearly indicate that the title compounds exhibit a block growth habit. Moreover, the constituent elements are uniformly distributed in single crystals from EDX element mapping analyses. The element contents were given in Fig. S2, indicating that the atomic percentage of Zn(Cd)/Ga/Te is about 1/2/4, which is consistent with the results of single crystal analyses.

#### 2.3. Optical characterizations

Based on the optical diffuse reflectance spectroscopy, the band gaps of title compounds are deduced by the Tauc plot method [52,53].

$$(\alpha h \upsilon)^{n} = A(h \upsilon - E_{g}) \tag{1}$$

where  $\alpha$  is the absorption coefficient proportional to F(R), h is Planck constant, v is light frequency, A is absorption constant,  $E_g$  is the optical band gap, n is the constant exponent that determines the type of optical transitions, and the value of n for indirect and direct transitions is 1/2 and 2, respectively. The absorption F(R) is determined by Kubelka-Munk transformation [54,55].

$$F(R) = \frac{K}{S} = \frac{(1 - R)^2}{2R}$$
 (2)

where K, S, and R represent the absorption, scattering, and reflectance, respectively. According to the Tauc method, the plots of  $(F(R)h\upsilon)^2$  and  $(F(R)h\upsilon)^{1/2}$  versus  $h\upsilon$  are exhibited in Fig. 3a and 3b to confirm whether the compounds are indirect or direct band gap semiconductors. The band gaps of  $ZnGa_2Te_4$  and  $ZnGa_2Te_4$  obtained from  $(F(R)h\upsilon)^2$  are 1.40 and 1.53 eV, respectively. However, the results deduced by the  $(F(R)h\upsilon)^{1/2}$  diagram are much smaller  $(E_g (ZnGa_2Te_4) = 1.17 \text{ eV}, E_g (CdGa_2Te_4) = 1.12 \text{ eV})$ . Fouad et al. demonstrated that  $ZnGa_2Te_4$  is an indirect band gap compound in 2011, and Ozaki et al. illustrated that  $ZnGa_2Te_4$  is a direct band gap semiconductor in 2003 [48,56]. Therefore, the band gaps of  $ZnGa_2Te_4$  and  $ZnGa_2Te_4$  are deduced as 1.17 eV and 1.53 eV, respectively. In fact, the band gap of  $ZnGa_2Te_4$  is wider than those of many known tellurides, such as  $ZnGa_2Te_4$  is wider than those of many known tellurides, such as  $ZnGa_2Te_4$  ( $ZnGa_2Te_4$ ) and  $ZnGa_2Te_4$  ( $ZnGa_2Te_4$ ) [44],  $ZnGa_2Te_4$  ( $ZnGa_2Te_4$ ) [56],  $ZnGa_2Te_4$  ( $ZnGa_2Te_4$ ) [44], and  $ZnGa_2Te_4$  ( $ZnGa_2Te_4$ ) [58].

Raman spectra of  $MGa_2Te_4$  (M=Zn, Cd) polycrystalline powder are recorded in Fig. 3c and 3d. Interestingly, the Raman diagrams of these compounds are similar because they are isostructural. The peaks between 190 and 410 cm<sup>-1</sup> can be attributed to the vibration modes of Zn/Cd-Te bond, while the peaks located at 637 and 755 cm<sup>-1</sup> in  $ZnGa_2Te_4$  and 637 and 746 cm<sup>-1</sup> in  $ZnGa_2Te_4$  are caused by the vibration of Zn-Te

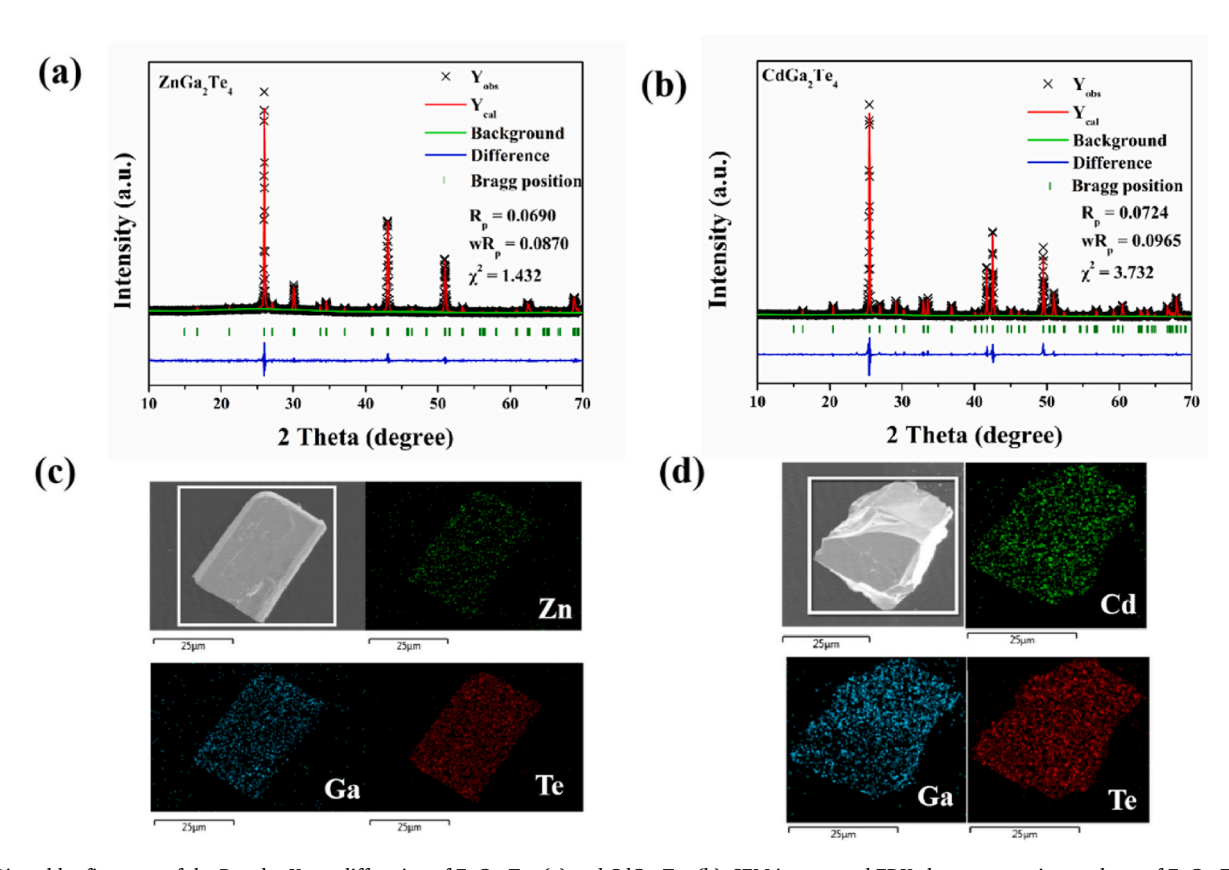


Fig. 2. Rietveld refinement of the Powder X-ray diffraction of ZnGa<sub>2</sub>Te<sub>4</sub> (a) and CdGa<sub>2</sub>Te<sub>4</sub> (b). SEM images and EDX element mapping analyses of ZnGa<sub>2</sub>Te<sub>4</sub> (c) and CdGa<sub>2</sub>Te<sub>4</sub> (d).

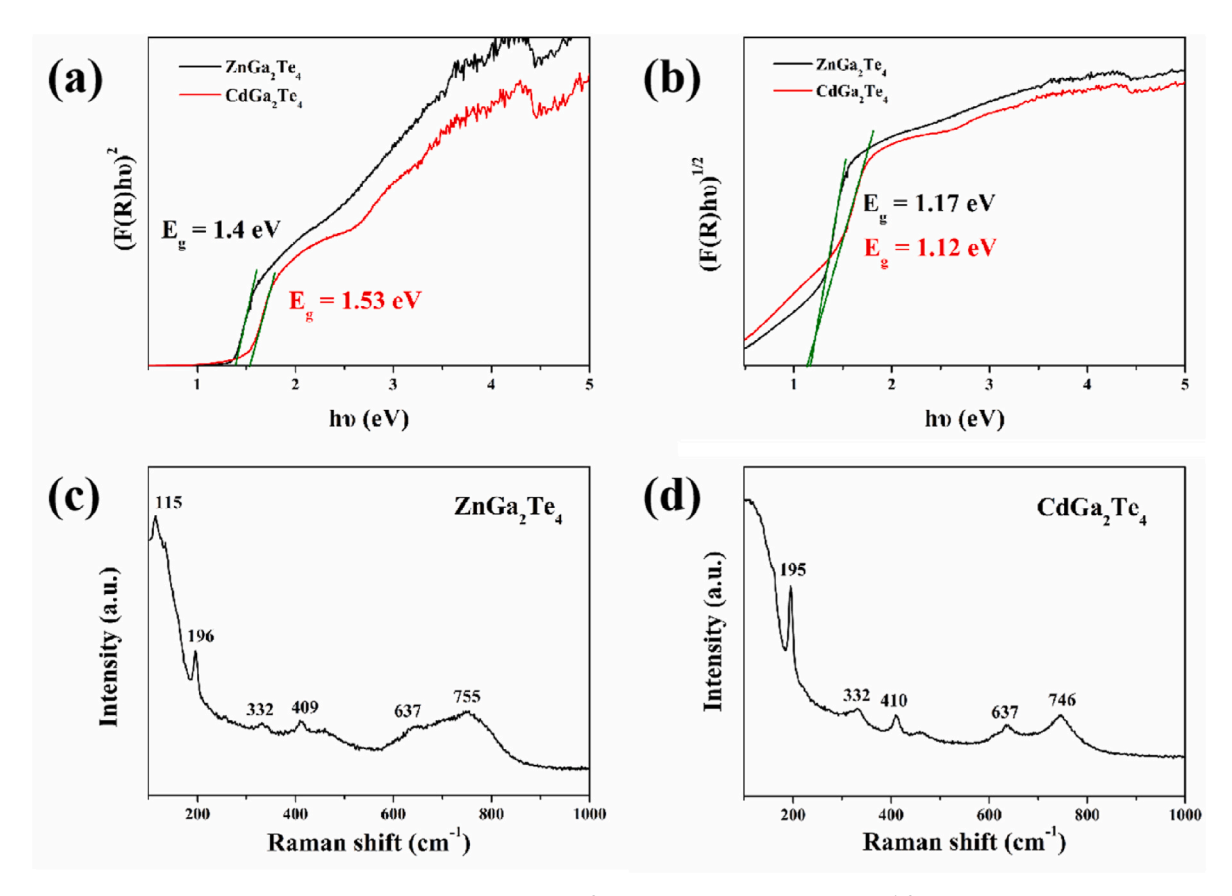


Fig. 3. UV-vis-NIR spectra of MGa<sub>2</sub>Te<sub>4</sub> (M = Zn, Cd). (a) the plot of  $(F(R)h\upsilon)^2$  versus  $h\upsilon$ ; (b) the plot of  $(F(R)h\upsilon)^{1/2}$  versus  $h\upsilon$ . The Raman spectra of ZnGa<sub>2</sub>Te<sub>4</sub> (c) and CdGa<sub>2</sub>Te<sub>4</sub> (d).

bonds [44,59]. The IR spectra are given in Fig. S3, except for the vibration peak of O-H at about 3500 cm $^{-1}$ , there is no obvious absorption peak.

### 2.4. Thermal analysis

The thermal behavior of title compounds was investigated by differential scanning calorimetry, and the results are exhibited in Fig. 4. There is one endothermic peak and one exothermic peak in CdGa<sub>2</sub>Te<sub>4</sub> compound, indicating that it has a melting point of 831 °C. In contrast, a very weak endothermic peak at 918 °C was detected in ZnGa<sub>2</sub>Te<sub>4</sub> compound, possibly indicating a 918 °C melting point. Moreover, the powder XRD patterns of MGa<sub>2</sub>Te<sub>4</sub> (M = Zn, Cd) after melting matched well with those before melting, implying that MGa<sub>2</sub>Te<sub>4</sub> (M = Zn, Cd)

possess congruent-melting behaviors (Fig. S4). Thereby, it is possible to grow large size single crystals using the Bridgman technique.

### 2.5. Powder SHG measurement

As MGa $_2$ Te $_4$  (M = Zn, Cd) crystallized in the non-centrosymmetric space group, their powder SHG intensities were recorded based Kurtz-Perry method. It can be seen that the SHG intensities of MGa $_2$ Te $_4$  (M = Zn, Cd) firstly increase with the particle size increasing, and then decrease gradually when the particle size reaches 90–125  $\mu$ m (Fig. 5a). The results demonstrate that the two compounds cannot achieve type-I phase matching. However, the declining trend of SHG intensity in CdGa $_2$ Te $_4$  is significantly lower than that of ZnGa $_2$ Te $_4$ , indicating that the former is closer to realizing phase-matching than the latter.

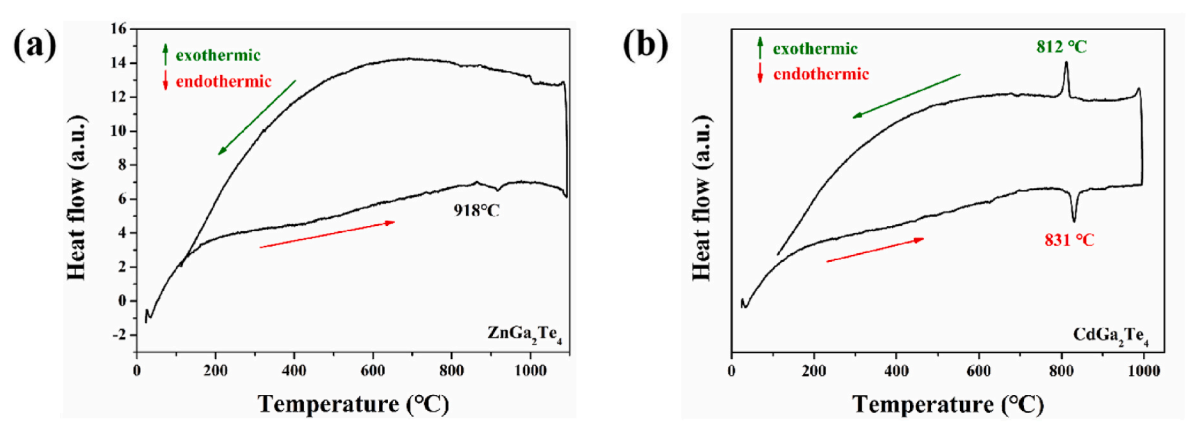


Fig. 4. Differential scanning calorimetry (DSC) curves of MGa<sub>2</sub>Te<sub>4</sub> (M = Zn, Cd).

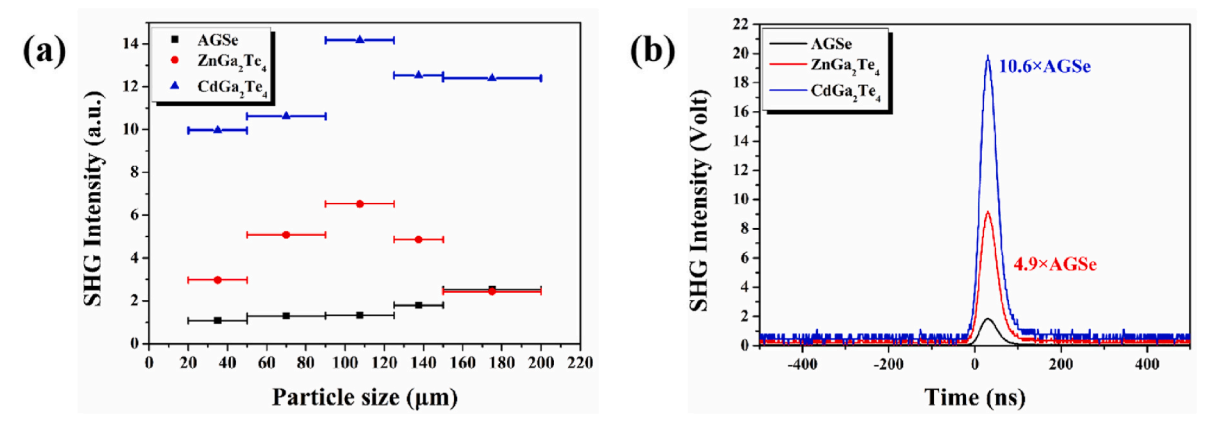


Fig. 5. (a) Size-dependent SHG intensities of  $MGa_2Te_4$  (M=Zn, Cd) and  $AgGaSe_2$  (as a reference) under 2090 nm radiation; (b) Oscilloscope traces of SHG signals for  $MGa_2Te_4$  (M=Zn, Cd) and  $AgGaSe_2$  at a particle size of 90-125  $\mu m$ .

Moreover, as shown in Fig. 5b, both  $ZnGa_2Te_4$  and  $CdGa_2Te_4$  possess strong SHG response of about 4.9 times and 10.6 times that of  $AgGaSe_2$  at 90–125  $\mu$ m, respectively, which is significantly larger than some known non-phase-matching IR NLO materials, such as  $Sm_4GaSbS_9$  (3.8  $\times$  AGS);  $La_4InSbS_4$  (1.5  $\times$  AGS);  $Eu_2Ga_2GeS_7$  (1.6  $\times$  AGS),  $Ba_5In_4S_7Te_4$  (0.5  $\times$  AGS),  $CsMn_4In_5Te_{12}$  (1.7  $\times$  AGS), and  $CsZn_4In_5Te_{12}$  (4.3  $\times$  AGS).

#### 2.6. Theoretical calculation

In order to figure out the relationship between structure and property, the First-principles calculations were performed to calculate the electronic structure and density of states of these two compounds, as shown in Fig. 6. The calculated band gaps of  $ZnGa_2Te_4$  and  $CdGa_2Te_4$  are 1.349 and 1.548 eV (Fig. 6a and 6b), respectively, which are very close to the experimental values shown in Fig. 3. Notably, although the two compounds are isostructural, their electronic structures differ slightly. Specifically, the valence band (VB) maximum of  $ZnGa_2Te_4$  is located at  $\Gamma$  point but the conduction band (CB) minimum is located at  $\Gamma$  point, indicating that it is an indirect band gap semiconductor, while the VB maximum and the CB minimum of  $CdGa_2Te_4$  are at  $\Gamma$  point, suggesting

that CdGa<sub>2</sub>Te<sub>4</sub> is a direct band gap semiconductor. Calculations of Mulliken bond order indices show that in ZnGa<sub>2</sub>Te<sub>4</sub>, the Te–Ga bonds are more covalent and Te–Zn bonds are more ionic. While in CdGa<sub>2</sub>Te<sub>4</sub>, the Te–Ga and Te–Cd bonds are more uniformly covalent (Fig. S5). This may be the main difference between these two crystals. Furthermore, the density of states (DOS) of both compounds are exhibited in Fig. 6c and 6d. The upper region of valence bands (VB) of ZnGa<sub>2</sub>Te<sub>4</sub> and CdGa<sub>2</sub>Te<sub>4</sub> consists of almost only Te 5*p* orbitals. The bottom region of conduction bands (CB) is mainly occupied by Te 6*p* and Ga 4*s* orbitals.

In addition, the NLO origin of compounds was qualitatively analyzed by the SHG-density method [60–63]. As shown in Fig. 7a and 7b, the SHG contribution of occupied states in  $\rm ZnGa_2Te_4$  and  $\rm CdGa_2Te_4$  originates from the non-bonded electrons of Te ions due to vacancies. By contrast, the lone-pair packet of  $\rm ZnGa_2Te_4$  is not only smaller than that of  $\rm CdGa_2Te_4$ , but the "green bubble" also indicates that the former is much more confined than the latter. In addition, the primary SHG contribution of empty states of  $\rm ZnGa_2Te_4$  comes from the "anti-cap" of lone-pair on Te ions (tilt toward  $\rm Ga\_Te\_Ga$  angle), with secondary contribution centered around those  $\rm Ga$  which are in the same plane with  $\rm Zn$  ions (Fig. 7c). In  $\rm CdGa_2Te_4$ , the role is reversed. As shown in Fig. 7d,

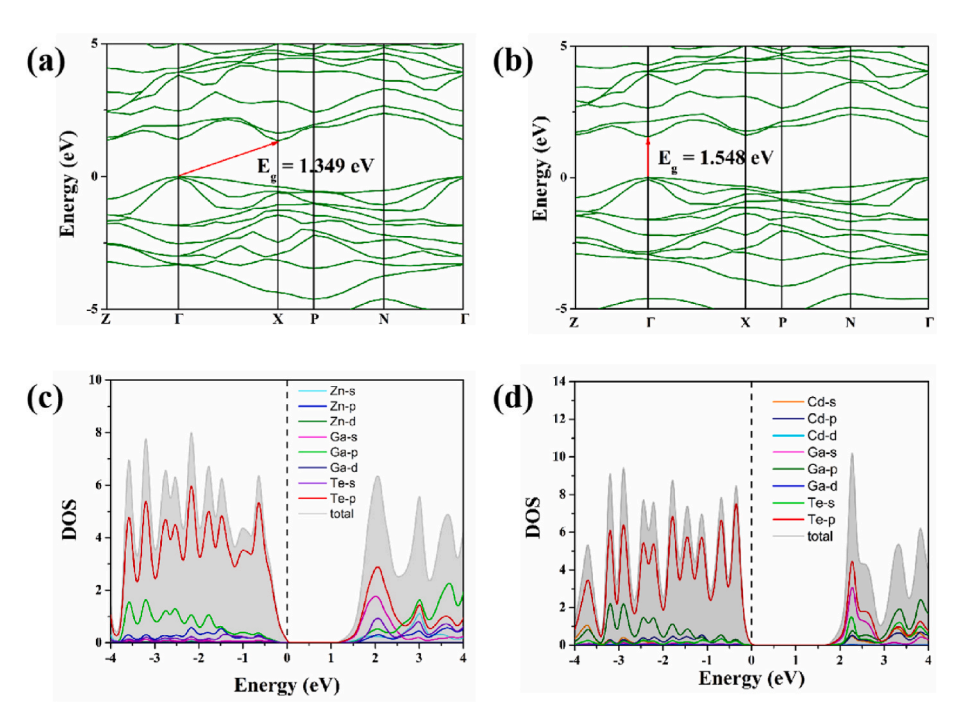


Fig. 6. Calculated band structure of ZnGa<sub>2</sub>Te<sub>4</sub> (a) and CdGa<sub>2</sub>Te<sub>4</sub> (b); Projected density of states of ZnGa<sub>2</sub>Te<sub>4</sub> (c) and CdGa<sub>2</sub>Te<sub>4</sub> (d).

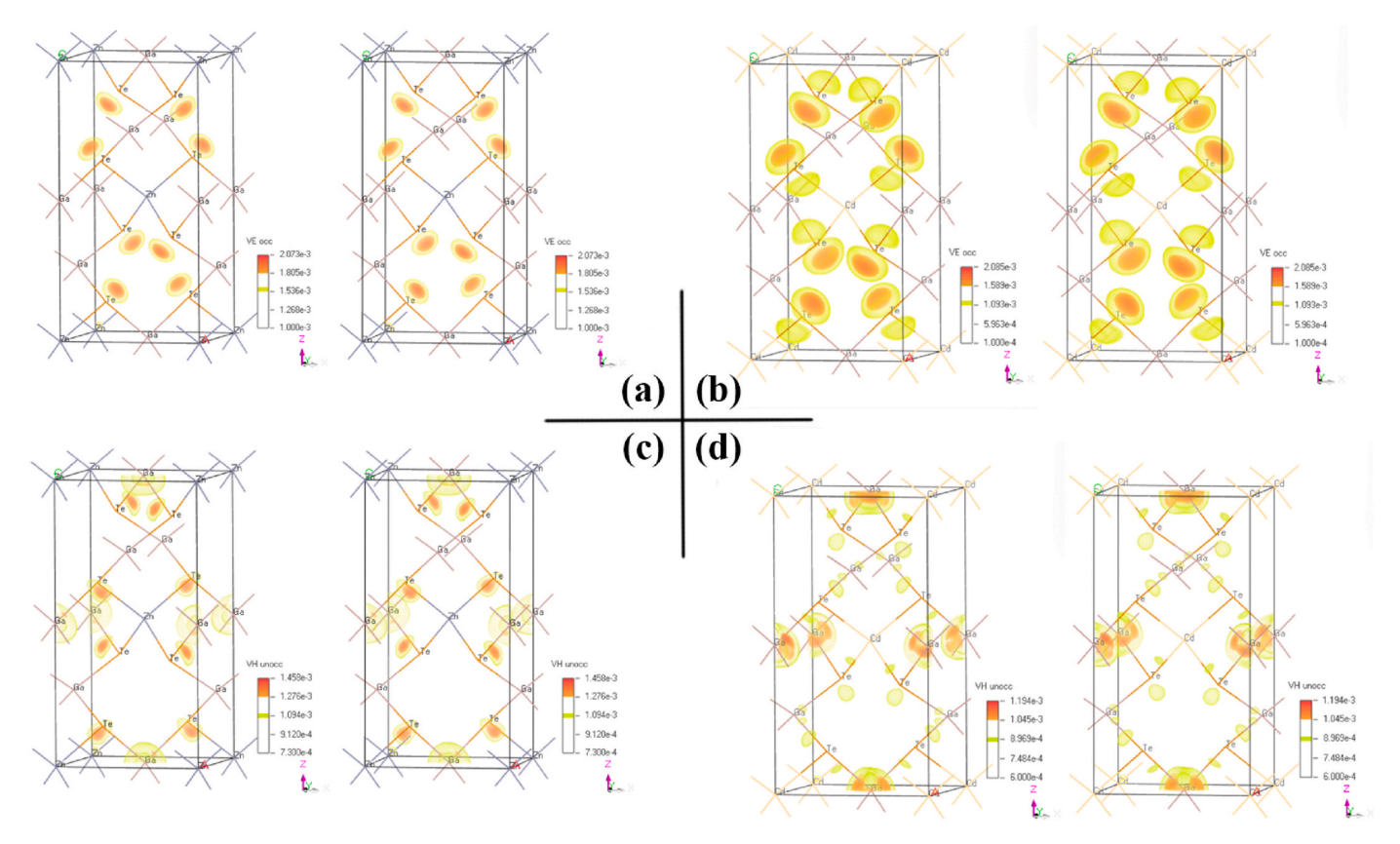


Fig. 7. Detail comparison of  $d_{14}$  SHG-densities virtual-electron occupied (VE occ) states of ZnGa<sub>2</sub>Te<sub>4</sub> (a) and CdGa<sub>2</sub>Te<sub>4</sub> (b) in cross-eyes stereo-pairs; Detail comparison of  $d_{14}$  SHG-densities virtual-hole unoccupied (VH unocc) states of ZnGa<sub>2</sub>Te<sub>4</sub> (c) and CdGa<sub>2</sub>Te<sub>4</sub> (d) in cross-eyes stereo-pairs. Here the maximum value and medium value is spanned in reverse rainbow scheme.

the major contribution comes from Ga, and the minor contribution originates from empty states near Te, as enclosed by "green bubble" (75% isosurface of maximum value), twin lopes near Te perpendicular to each Cd–Te bonds. In general, the electron cloud in CdGa<sub>2</sub>Te<sub>4</sub> is widely distributed, so it is more cooperative and collective in the structural framework, which makes CdGa<sub>2</sub>Te<sub>4</sub> more covalent. In contrast, the electron cloud in ZnGa<sub>2</sub>Te<sub>4</sub> is more concentrated, so it is more isolated and localized in the structural framework, which leads to ZnGa<sub>2</sub>Te<sub>4</sub> more ionic.

Furthermore, the SHG coefficients were calculated for the crystal structures in both conventional cell and primitive cell (Figs. S6-S7) for comparison, and the results were given in Tables S6-S7. They show the results of ZnGa<sub>2</sub>Te<sub>4</sub> and CdGa<sub>2</sub>Te<sub>4</sub> from both sum-over-states optical properties calculations and E-field DFPT calculations, respectively. According to the restriction of Kleinman symmetry, MGa<sub>2</sub>Te<sub>4</sub> (M = Zn, Cd) possesses three non-zero independent second-order tensors ( $d_{14}$ ,  $d_{15}$ , and  $d_{21}$ ). Notably, the  $d_{ii}$  obtained by the two methods are not consistent, but the ones calculated by the E-field method are more credible (after all, sum-over-states method is zero-order perturbation, and DFPT is linear response, that is, first-order perturbation) [17]. Therefore, taking crystal structure in primitive form based on E-field DFPT as an example, the calculated values of  $d_{14}$ ,  $d_{15}$ , and  $d_{21}$  are 127.67, -18.85, 18.85 pm/V for  $ZnGa_2Te_4$  and 105.19, -23.05, 23.05 pm/V for CdGa<sub>2</sub>Te<sub>4</sub>, respectively, which are in good agreement with the experimental results. Notably, although the calculated  $d_{14}$  value of ZnGa<sub>2</sub>Te<sub>4</sub> is slightly larger than that of CdGa<sub>2</sub>Te<sub>4</sub>, the results of SHG measurement are quite the opposite. The reason for this phenomenon may be that the corresponding wavelength of the band gap ZnGa2Te4 are close to the second harmonic wavelength of 1045 nm, which leads to stronger absorption of the second-harmonic light than CdGa<sub>2</sub>Te<sub>4</sub> [64]. Therefore, the influence of the band gap on the SHG result is very significant. A

similar situation can be observed in  $Ba_2Ge_2Te_5$ - the band gap of  $Ba_2Ge_2Te_5$  is 1.15~eV, and the measured SHG intensity is about 0.45 times that of AGS while the theoretical NLO coefficient is about 16 times that of AGS [57]. Besides, the birefringence of two compounds were also calculated. The results on birefringence in conventional form are consistent between these two methods, while the birefringence results in primitive form calculated by SOS optics method are slightly smaller than those by E-field method.

The calculated refractive index dispersion curves of the two compounds were depicted in Fig. 8. The results indicated that MGa<sub>2</sub>Te<sub>4</sub> (M = Zn, Cd) are positive uniaxial crystals and their birefringence values are 0.016 and 0.018@2090 nm, respectively. Admittedly, such birefringence is smaller than that of some known tellurides [43,44,65]. It is likely that the distortion magnitudes (△d) of ZnTe<sub>4</sub>/CdTe<sub>4</sub> and GaTe<sub>4</sub> tetrahedra are calculated to be 0, which leads to the decrease of structural optical anisotropy. Furthermore, the shortest SHG phase-matching wavelengths of ZnGa<sub>2</sub>Te<sub>4</sub> and CdGa<sub>2</sub>Te<sub>4</sub> were deduced to be 3300 nm and 2950 nm, respectively, as shown in Fig. 8c and 8d. This means that Type-I phase-matching cannot be achieved using a 2090 nm laser as the fundamental frequency light, which is consistent with the experimental SHG results. Perhaps we can focus on other types of NLO techniques. Therefore, it is reasonable to expect that ZnGa<sub>2</sub>Te<sub>4</sub> and CdGa<sub>2</sub>Te<sub>4</sub> might successfully achieve phase-matching behavior via OPO technology. In addition, the use of phase-mismatch in the NLO crystal as a phase modulation mechanism for generating transform-limited femtosecond optical pulses also has important application prospects. The phase modulation caused by phase-mismatch between ZnGa2Te4 and CdGa<sub>2</sub>Te<sub>4</sub> can be realized in other types of nonlinear resonators, facilitating the development of novel femtosecond pulses frequency-comb sources.

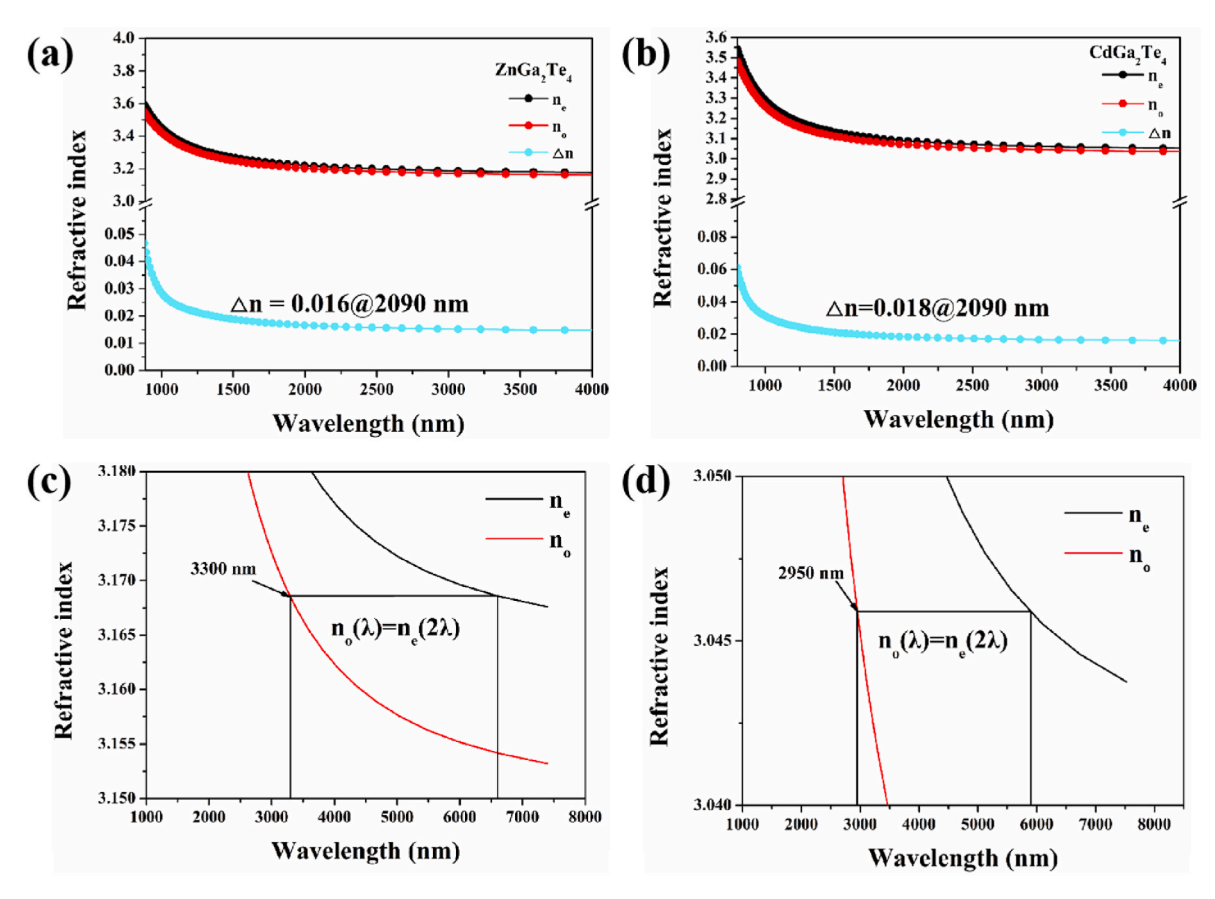


Fig. 8. Calculated refractive index dispersion curves of  $ZnGa_2Te_4$  (a) and  $CdGa_2Te_4$  (b); The shortest SHG phase-matching wavelength of  $ZnGa_2Te_4$  (c) and  $CdGa_2Te_4$  (d).

### 3. Conclusion

In summary, two defect DL tellurides MGa<sub>2</sub>Te<sub>4</sub> (M = Zn, Cd) were successfully synthesized, which can also be derived from DL-type AgGaS2 by adjusting the Ag ion. This is the first comprehensive study of IR NLO properties and insightful structural properties of MGa<sub>2</sub>Te<sub>4</sub>. Experimental results demonstrate that both compounds exhibit moderate band gap, strong SHG response, about 4.9-10.6 × AGSe@90-125 μm. Besides, MGa<sub>2</sub>Te<sub>4</sub> (M = Zn, Cd) melts congruently, enabling the facile growth of large single crystals. Furthermore, SHG coefficients calculations using primitive cell based on E-field DFPT method indicate tremendous SHG tensors (127.67 pm/V for ZnGa<sub>2</sub>Te<sub>4</sub>, 105.19 pm/V for CdGa<sub>2</sub>Te<sub>4</sub>), which are significantly larger than that of AgGaSe<sub>2</sub> ( $d_{36} = 36$ pm/V). To the best of our knowledge, it is rare in literature to demonstrate the consistency of primitive and conventional cell and compare linear and nonlinear optical properties using different theoretical methods. In addition, SHG-density analysis reveals that the giant SHG responses stem from the lone-pair packet of Te ions in [GaTe<sub>4</sub>] units. Therefore, our study not only provides an efficient access for the search of new NLO materials, but also shed light on future theoretical calculations.

### 4. Experimental

### 4.1. Single crystal synthesis

All starting materials, Zn (99.99%), Cd (99.99%), Ga (99.999%), and Te (99.9%) were directly purchased from Aladdin Co., Ltd. without further purification. The synthesis of binary materials ZnTe, CdTe, and  $Ga_2Te_3$  was to heat the stoichiometric mixture of the elements in vacuum flame-sealed silica tubes. All manipulations were carried out in an

Ar-filled glove box with O2 and H2O contents less than 0.1 ppm.

Single crystals of  $ZnGa_2Te_4$  and  $CdGa_2Te_4$  were grown via spontaneously crystallization. 0.1 g (0.518 mmol)/0.124 g (0.518 mmol) ZnTe/CdTe and 0.271 g (0.518 mmol)  $Ga_2Te_3$  were thoroughly ground and loaded into quartz tubes for the growth of  $ZnGa_2Te_4$  and  $CdGa_2Te_4$ , respectively. There tubes were slowly heated to 1123 K for  $ZnGa_2Te_4$  and 1173 K for  $ZnGa_2Te_4$  within 17 h and held for 50 h, then gradually cooled to 773 K at a rate of 3 K/h, and finally the furnaces were turned off. The metallic luster block-liked crystals of  $ZnGa_2Te_4$  (M = Zn, Cd) can be obtained after washed with deionized water. Both compounds can be stable in the ambient for several months.

### 4.2. Elemental analysis

The FEI Quanta 650FEG scanning electron microscope (SEM) equipped with Energy Dispersive X-ray (EDX) was used to perform the elemental content analysis and distribution on the single crystals of  $MGa_2Te_4$  (M = Zn, Cd).

### 4.3. Powder X-ray diffraction and rietveld refinement

A Bruker D8 Focus diffractometer equipped with Cu-K $_{\alpha}$  ( $\lambda=1.5418$  Å) radiation was used to perform the powder X-ray diffraction of MGa $_2$ Te $_4$  (M = Zn, Cd). The diffraction patterns from  $10^{\circ}$  to  $70^{\circ}$  were collected with the parameters of a scanning step width of  $0.02^{\circ}$  and a counting time of 0.2 s/step. Rietveld refinements using the collected powder X-ray diffraction data were carried out using the GSAS software package with the EXPGUI interface.

#### 4.4. Optical characterizations

A Carry 7000 UV–vis–NIR spectrophotometer was applied to obtain the diffuse-reflectance spectra of  $MGa_2Te_4\ (M=Zn,\ Cd)$  in the range of  $2500-200\ nm$  (polytetrafluoroethylene as a reference). A Lab RAM Aramis spectrometer equipped with a 532 nm laser was used to collect the Raman spectra of  $MGa_2Te_4\ (M=Zn,\ Cd)$  in the range of 1000 to 100 cm $^{-1}$  at room temperature. An Excalibur 3100 Fourier Transform Infrared Spectrometer collects the IR spectra in the range of 4000–400 cm $^{-1}$ .

### 4.5. Thermal properties

A Labsys TG-DTA16 (SETARAM) thermal analyzer was used to evaluate the thermal stability of  $MGa_2Te_4$  (M = Zn, Cd). Appropriate amount of  $MGa_2Te_4$  (M = Zn, Cd) polycrystalline powder was placed into quartz tubes with the size of 5 mm (o.d.)  $\times$  3 mm (i.d.) and eventually sealed the tubes at  $10^{-6}$  Pa. During the measurement process, the nitrogen flow was circulated at a flow rate of about 15 mL/min, and the temperature of the tube was heated from room temperature to 1273 K at a rate of 15 K/min.

### 4.6. Second harmonic generation measurement

The SHG intensities of  $MGa_2Te_4$  (M=Zn, Cd) were estimated by Kurtz-Perry technique with a 2090 nm laser generated by a Q-switch Ho: Tm:Cr:YAG laser [66]. The powder of  $MGa_2Te_4$  (M=Zn, Cd) was sieved into five particle ranges, namely 20–50, 50–90, 90–125, 125–150, and 150–200  $\mu m$ , and then these samples of different particle sizes were load into custom holders with a thickness of 0.5 mm. In addition, the microcrystals of the traditional material AGSe were sieved to the same particle ranges as mentioned above for reference.

### 4.7. Theoretical calculations

The First-principles Calculations were performed by the method of plane-wave pseudopotential in the CASTEP package according to density functional theory (DFT) [67-69]. The Perdew-Burke-Ernzerhof (PBE) function was used to describe the exchange-related energy in the generalized gradient approximation (GGA) with a 800 eV kinetic energy cutoff. The Q<sub>c</sub>-tuning type Optimized Norm-conserving Pseudopotential was chosen to simulate the interaction between the atom cores and the valence electrons with a small plane-wave basis [70–72], where the valence electrons configuration treated as Zn 3d<sup>10</sup>4s<sup>1.27</sup>4p<sup>0.73</sup>. Cd  $4d^{10}5s^{0.75}5p^{0.25}$ , Ga  $3d^{10}4s^24p^1$ , Te  $5s^25p^4$ . A very dense Monkhorst-Pack k-point mesh with grid spacing 0.03 Å were used to ensure convergence of conventional and primitive cells of ZnGa<sub>2</sub>Te<sub>4</sub> and CdGa<sub>2</sub>Te<sub>4</sub> in the numerically integration of the Brillouin zone, respectively. To calculate birefringence and SHG coefficient, both methods available to CASTEP were used, one based on a sum-over-states [73,74] type formalism referred as optical properties calculation, another based on E-field DFPT [75,76] perturbation recently implemented within CASTEP.

### Credit author statement

Mengran Sun: investigated and curated the data, designed and performed the experiments. Wrote the manuscript. Chunxiao Li: performed the SHG experiments. Jinlong Shi: investigated and curated the data. Ming-Hsien Lee: designed and performed the calculations. Wrote the manuscript. Jiyong Yao: designed and performed the experiments. Writing - original draft. All authors contributed to interpreting the results and commented on the manuscript.

#### **Declaration of competing interest**

The authors declare that they have no known competing financial interests or personal relationships that could have appeared to influence the work reported in this paper.

### Data availability

Data will be made available on request.

### Acknowledgements

This research was supported by the National Natural Science Foundation of China (22175190, 51890862). Thanks to Dr. Jian Tang at Institute of Chemical Materials, China Academy of Engineering Physics for the differential scanning calorimetry measurements.

### Appendix A. Supplementary data

Supplementary data to this article can be found online at https://doi.org/10.1016/j.mtphys.2023.101166.

### References

- P.S. Halasyamani, J.M. Rondinelli, The must-have and nice-to-have experimental and computational requirements for functional frequency doubling deep-UV crystals, Nat. Commun. 9 (1) (2018) 2972.
- [2] C. Chen, T. Sasaki, R. Li, Y. Wu, Z. Lin, Y. Mori, Z. Hu, J. Wang, G. Aka, M. Yoshimura, Nonlinear Optical Borate Crystals: Principals and Applications, John Wiley & Sons, 2012.
- [3] B. Ferguson, X.-C. Zhang, Materials for terahertz science and technology, Nat. Mater. 1 (1) (2002) 26–33.
- [4] M. Mutailipu, M. Zhang, Z. Yang, S. Pan, Targeting the next generation of deepultraviolet nonlinear optical materials: expanding from borates to borate fluorides to fluorooxoborates. Accounts Chem. Res. 52 (3) (2019) 791–801.
- [5] C. Chen, Y. Wang, B. Wu, K. Wu, W. Zeng, L. Yu, Design and synthesis of an ultraviolet-transparent nonlinear optical crystal Sr<sub>2</sub>Be<sub>2</sub>B<sub>2</sub>O<sub>7</sub>, Nature 373 (6512) (1995) 322–324.
- [6] J. Li, W.-D. Yao, J.-N. Li, X.-H. Li, W. Liu, S.-P. Guo, Partial substitution induced structural transformation and enhanced nonlinear optical properties of Na<sub>2</sub>Ga<sub>x</sub>In<sub>6</sub> <sub>x</sub>Se<sub>10</sub> (x = 3, 3.76), Mater. Today Phys. 32 (2023): 101007.
- [7] H. Chen, W.-B. Wei, H. Lin, X.-T. Wu, Transition-metal-based chalcogenides: a rich source of infrared nonlinear optical materials, Coord. Chem. Rev. 448 (2021): 214154.
- [8] E. Goulielmakis, M. Schultze, M. Hofstetter, V.S. Yakovlev, J. Gagnon, M. Uiberacker, A.L. Aquila, E. Gullikson, D.T. Attwood, R. Kienberger, Single-cycle nonlinear optics, Science 320 (5883) (2008) 1614–1617.
- [9] B. Guo, Y. Wang, C. Peng, H. Zhang, G. Luo, H. Le, C. Gmachl, D. Sivco, M. Peabody, A.Y. Cho, Laser-based mid-infrared reflectance imaging of biological tissues, Opt. Express 12 (1) (2004) 208–219.
- [10] J.-H. Zhao, X.-B. Li, Q.-D. Chen, Z.-G. Chen, H.-B. Sun, Ultrafast laser-induced black silicon, from micro-nanostructuring, infrared absorption mechanism, to high performance detecting devices, Mater. Today Nano 11 (2020): 100078.
- [11] M.-Y. Ran, A.Y. Wang, W.-B. Wei, X.-T. Wu, H. Lin, Q.-L. Zhu, Recent progress in the design of IR nonlinear optical materials by partial chemical substitution: structural evolution and performance optimization, Coord. Chem. Rev. 481 (2023): 215059
- [12] A.V. Munde, B.B. Mulik, R.P. Dighole, S.C. Dhawale, L.S. Sable, A.T. Avhale, B. R. Sathe, Bi<sub>2</sub>O<sub>3</sub>@ Bi nanoparticles for ultrasensitive electrochemical determination of thiourea: monitoring towards environmental pollutants, Electrochim. Acta 394 (2021): 139111.
- [13] A. Okorogu, S. Mirov, W. Lee, D. Crouthamel, N. Jenkins, A.Y. Dergachev, K. Vodopyanov, V. Badikov, Tunable middle infrared downconversion in GaSe and AgGaS<sub>2</sub>, Opt Commun. 155 (4–6) (1998) 307–312.
- [14] G. Boyd, H. Kasper, J. McFee, F. Storz, Linear and nonlinear optical properties of some ternary selenides, IEEE J. Quant. Electron. 8 (12) (1972) 900–908.
- [15] G. Boyd, E. Buehler, F. Storz, Linear and nonlinear optical properties of ZnGeP<sub>2</sub> and CdSe, Appl. Phys. Lett. 18 (7) (1971) 301–304.
- [16] C. Li, Y. Liu, W. Liu, J. Liu, X. Meng, Z. Lin, J. Yao, Cd<sub>7</sub>SiAs<sub>6</sub>, A nonchalcopyrite arsenide with a strong nonlinear-optical response, Inorg. Chem. 60 (24) (2021) 18634–18638.
- [17] M. Sun, W. Xing, M.-H. Lee, J. Yao, Bridging oxygen atoms in trigonal prism units driven strong second-harmonic-generation efficiency in Sr<sub>3</sub>Ge<sub>2</sub>O<sub>4</sub>Te<sub>3</sub>, Chem. Commun. 58 (79) (2022) 11167–11170.
- [18] M. Zhou, Y. Yang, Y. Guo, Z. Lin, J. Yao, Y. Wu, C. Chen, Hg-based infrared nonlinear optical material KHg<sub>4</sub>Ga<sub>5</sub>Se<sub>12</sub> exhibits good phase-matchability and exceptional second harmonic generation response, Chem. Mater. 29 (18) (2017) 7993–8002.

- [19] I. Chung, M.G. Kanatzidis, Metal chalcogenides: a rich source of nonlinear optical materials, Chem. Mater. 26 (1) (2014) 849–869.
- [20] C. Li, X. Meng, Z. Li, J. Yao, Hg-based chalcogenides: an intriguing class of infrared nonlinear optical materials, Coord. Chem. Rev. 453 (2022): 214328.
- [21] F. Liang, L. Kang, Z. Lin, Y. Wu, C. Chen, Analysis and prediction of mid-IR nonlinear optical metal sulfides with diamond-like structures, Coord. Chem. Rev. 333 (2017) 57–70.
- [22] Z. Li, J. Yao, Y. Wu, Chalcophosphates: a treasure house of infrared nonlinear optical materials, Cryst. Growth Des. 20 (11) (2020) 7550–7564.
- [23] Z. Li, S. Zhang, Z. Huang, L.-D. Zhao, E. Uykur, W. Xing, Z. Lin, J. Yao, Y. Wu, Molecular construction from AgGaS<sub>2</sub> to CuZnPS<sub>4</sub>: defect-induced second harmonic generation enhancement and cosubstitution-driven band gap enlargement, Chem. Mater. 32 (7) (2020) 3288–3296.
- [24] Y. Guo, F. Liang, J. Yao, Z. Lin, W. Yin, Y. Wu, C. Chen, Nonbonding electrons driven strong SHG effect in Hg<sub>2</sub>GeSe<sub>4</sub>: experimental and theoretical investigations, Inorg. Chem. 57 (12) (2018) 6795–6798.
- [25] V. Petrov, A. Yelisseyev, L. Isaenko, S. Lobanov, A. Titov, J.-J. Zondy, Second harmonic generation and optical parametric amplification in the mid-IR with orthorhombic biaxial crystals LiGaS<sub>2</sub> and LiGaSe<sub>2</sub>, Appl. Phys. B 78 (2004) 543–546.
- [26] G.D. Boyd, H.M. Kasper, J.H. McFee, Linear and nonlinear optical properties of LilnS<sub>2</sub>, J. Appl. Phys. 44 (6) (1973) 2809–2812.
- [27] J.W. Lekse, M.A. Moreau, K.L. McNerny, J. Yeon, P.S. Halasyamani, J.A. Aitken, Second-harmonic generation and crystal structure of the diamond-like semiconductors Li<sub>2</sub>CdGeS<sub>4</sub> and Li<sub>2</sub>CdSnS<sub>4</sub>, Inorg. Chem. 48 (16) (2009) 7516, 7518
- [28] J.A. Brant, D.J. Clark, Y.S. Kim, J.I. Jang, A. Weiland, J.A. Aitken, Outstanding laser damage threshold in Li<sub>2</sub>MnGeS<sub>4</sub> and tunable optical nonlinearity in diamondlike semiconductors, Inorg. Chem. 54 (6) (2015) 2809–2819.
- [29] K.P. Devlin, A.J. Glaid, J.A. Brant, J.-H. Zhang, M.N. Srnec, D.J. Clark, Y.S. Kim, J. I. Jang, K.R. Daley, M.A. Moreau, Polymorphism and second harmonic generation in a novel diamond-like semiconductor: Li<sub>2</sub>MnSnS<sub>4</sub>, J. Solid State Chem. 231 (2015) 256–266.
- [30] A. Weiland, J.-H. Zhang, D.J. Clark, J.A. Brant, C.W. Sinagra, Y.S. Kim, J.I. Jang, J. A. Aitken, Correction: infrared nonlinear optical properties of lithium-containing diamond-like semiconductors Li<sub>2</sub>ZnGeSe<sub>4</sub> and Li<sub>2</sub>ZnSnSe<sub>4</sub>, Dalton Trans. 46 (30) (2017) 10102–10104.
- [31] J.-H. Zhang, D.J. Clark, J.A. Brant, C.W. Sinagra, Y.S. Kim, J.I. Jang, J.A. Aitken, Infrared nonlinear optical properties of lithium-containing diamond-like semiconductors Li<sub>2</sub> ZnGeSe<sub>4</sub> and Li<sub>2</sub>ZnSnSe<sub>4</sub>, Dalton Trans. 44 (24) (2015) 11212–11222.
- [32] G.M. Ford, Q. Guo, R. Agrawal, H.W. Hillhouse, Earth abundant element  $Cu_2Zn$   $(Sn_{1-x}Ge_x)S_4$  nanocrystals for tunable band gap solar cells: 6.8% efficient device fabrication, Chem. Mater. 23 (10) (2011) 2626–2629.
- [33] K.A. Rosmus, J.A. Brant, S.D. Wisneski, D.J. Clark, Y.S. Kim, J.I. Jang, C. D. Brunetta, J.-H. Zhang, M.N. Srnec, J.A. Aitken, Optical nonlinearity in Cu<sub>2</sub>CdSnS<sub>4</sub> and α/β-Cu<sub>2</sub>ZnSiS<sub>4</sub>: diamond-like semiconductors with high laser-damage thresholds, Inorg. Chem. 53 (15) (2014) 7809–7811.
- [34] A. Abudurusuli, J. Huang, P. Wang, Z. Yang, S. Pan, J. Li, Li<sub>4</sub>MgGe<sub>2</sub>S<sub>7</sub>: the first alkali and alkaline-earth diamond-like infrared nonlinear optical material with exceptional large band gap, Angew. Chem. Int. Ed. 60 (45) (2021) 24131–24136.
- [35] E. Parthé, Crystal Chemistry of Tetrahedral Structures, CRC Press, 1964.
- [36] B. Levine, C. Bethea, H. Kasper, F. Thiel, Nonlinear optical susceptibility of HgGa<sub>2</sub>S<sub>4</sub>, IEEE J. Quant. Electron. 12 (6) (1976) 367–368.
- [37] W. Jantz, P. Koidl, W. Wettling, Elastic, optical and nonlinear optical properties of InPS<sub>4</sub>, Appl. Phys. A 30 (1983) 109–115;
   [a] Y. Chu, P. Wang, H. Zeng, S. Cheng, X. Su, Z. Yang, J. Li, Pan, S., Hg3P2S8: a new promising infrared nonlinear optical material with a large second-harmonic generation and a high laser-induced damage threshold, Chem. Mater. 33 (16) (2021) 6514–6521.
- [38] Y. Chu, P. Wang, H. Zeng, S. Cheng, X. Su, Z. Yang, J. Li, S. Pan, Hg<sub>3</sub>P<sub>2</sub>S<sub>8</sub>: a new promising infrared nonlinear optical material with a large second-harmonic generation and a high laser-induced damage threshold, Chem. Mater. 33 (16) (2021) 6514–6521.
- [39] P. Wang, Y. Chu, A. Tudi, C. Xie, Z. Yang, S. Pan, J. Li, The combination of structure prediction and experiment for the exploration of alkali-earth metalcontained chalcopyrite-like IR nonlinear optical material, Adv. Sci. 9 (15) (2022): 2106120.
- [40] M. Zhou, L. Kang, J. Yao, Z. Lin, Y. Wu, C. Chen, Midinfrared nonlinear optical thiophosphates from LiZnPS<sub>4</sub> to AgZnPS<sub>4</sub>: a combined experimental and theoretical study, Inorg. Chem. 55 (8) (2016) 3724–3726.
- [41] W. Xing, N. Wang, C. Tang, C. Li, Z. Lin, J. Yao, W. Yin, B. Kang, From AgGaS<sub>2</sub> to AgHgPS<sub>4</sub>: vacancy defects and highly distorted HgS<sub>4</sub> tetrahedra double-induced remarkable second-harmonic generation response, J. Mater. Chem. C 9 (3) (2021) 1062–1068.
- [42] M. Sun, X. Zhang, C. Li, W. Liu, Z. Lin, J. Yao, Highly polarized [GeOTe<sub>3</sub>] motifdriven structural order promotion and an enhanced second harmonic generation response in the new nonlinear optical oxytelluride Ba<sub>3</sub>Ge<sub>2</sub>O<sub>4</sub>Te<sub>3</sub>, J. Mater. Chem. C 10 (1) (2022) 150–159.
- [43] M. Sun, X. Zhang, W. Xing, E. Uykur, W. Yin, Z. Lin, J. Yao, Ba<sub>6</sub>In<sub>2</sub>Ge<sub>2</sub>Te<sub>15</sub>: a THz birefringent material with an intriguing quasi-[Te<sub>5</sub>]<sup>4-</sup> chain possessing large optical anisotropy and an ultrawide transmission range, Inorg. Chem. Front. 9 (14) (2022) 3421–3427.
- [44] M. Sun, X. Zhang, W. Xing, Z. Li, W. Liu, Z. Lin, W. Yin, J. Yao, Synthesis and characterizations of two tellurides  $\beta$ -Baga<sub>2</sub>Te<sub>4</sub> and Ba<sub>5</sub>Ga<sub>2</sub>Ge<sub>3</sub>Te<sub>12</sub> with flexible chain structure, Inorg. Chem. 60 (19) (2021) 14793–14802.

- [45] P.G. Schunemann, S.D. Setzler, T.M. Pollak, M.C. Ohmer, J.T. Goldstein, D. E. Zelmon, Crystal growth and properties of AgGaTe<sub>2</sub>, J. Cryst. Growth 211 (1) (2000) 242–246.
- [46] S. Zhang, F. Liang, P. Gong, Y. Yang, Z. Lin, Na<sub>4</sub>CdGe<sub>2</sub>S<sub>7</sub>: a sodium-rich quaternary wide-band-gap chalcogenide with two-dimensional [Ge<sub>2</sub>CdS<sub>7</sub>]∞ Layers, Inorg. Chem. 59 (22) (2020) 16132–16136.
- [47] H. Hahn, G. Frank, W. Klingler, A.D. Störger, G. Störger, Untersuchungen über ternäre chalkogenide. VI. Über Ternäre chalkogenide des aluminiums, galliums und indiums mit Zink, cadmium und quecksilber, Z. Anorg. Allg. Chem. 279 (5–6) (1955) 241–270.
- [48] S. Fouad, G. Sakr, I. Yahia, D.A. Basset, Structural characterization and novel optical properties of defect chalcopyrite ZnGa<sub>2</sub>Te<sub>4</sub> thin films, Mater. Res. Bull. 46 (11) (2011) 2141–2146.
- [49] P. Kumar, A. Soni, K. Bhamu, J. Sahariya, Optoelectronic behavioral study of defect-chalcopyrite semiconductors XGa<sub>2</sub>Te<sub>4</sub> (X= Zn, Cd), Mater. Res. Bull. 86 (2017) 131–138.
- [50] P. Govindaraj, M. Sivasamy, K. Murugan, K. Venugopal, P. Veluswamy, Pressuredriven thermoelectric properties of defect chalcopyrite structured ZnGa<sub>2</sub>Te<sub>4</sub>: ab initio study, RSC Adv. 12 (20) (2022) 12573–12582.
- [51] H. Liu, D. Tian, Z. Du, J. Cui, Coexisting transport behaviors in quasibinary Cd<sub>(3-3m)</sub>Ga<sub>2m</sub>Te<sub>3</sub> (m= 0.75-0.98) system with structural vacancy and cationic interdiffusion, Scripta Mater. 113 (2016) 194–197.
- [52] C. Aydin, M. Benhaliliba, A.A. Al-Ghamdi, Z.H. Gafer, F. El-Tantawy, F. Yakuphanoglu, Determination of optical band gap of ZnO: ZnAl<sub>2</sub>O<sub>4</sub> composite semiconductor nanopowder materials by optical reflectance method, J. Electroceram. 31 (2013) 265–270.
- [53] F. Yakuphanoglu, S. Ilican, M. Caglar, Y. Caglar, The determination of the optical band and optical constants of non-crystalline and crystalline ZnO thin films deposited by spray pyrolysis, J. Optoelectron. Adv. Mater. 9 (7) (2007) 2180.
- [54] C. Aydin, M. Abd El-sadek, K. Zheng, I. Yahia, F. Yakuphanoglu, Synthesis, diffused reflectance and electrical properties of nanocrystalline Fe-doped ZnO via solgel calcination technique, Opt Laser. Technol. 48 (2013) 447–452.
- [55] E. Simmons, Diffuse reflectance spectroscopy: a comparison of the theories, Appl. Opt. 14 (6) (1975) 1380–1386.
- [56] S. Ozaki, K.-i. Muto, S. Adachi, Optical properties and electronic band structure of CdGa<sub>2</sub>Te<sub>4</sub>, J. Phys. Chem. Solid. 64 (9–10) (2003) 1935–1939.
- [57] M.-Y. Ran, Z. Ma, X.-T. Wu, H. Lin, Q.-L. Zhu, Ba<sub>2</sub>Ge<sub>2</sub>Te<sub>5</sub>: a ternary NLO-active telluride with unusual one-dimensional helical chains and giant second harmonic-generation tensors, Inorg. Chem. Front. 8 (22) (2021) 4838–4845.
- [58] S.A. Avanesov, D.V. Badikov, V.V. Badikov, V.L. Panyutin, V. Petrov, G. S. Shevyrdyaeva, A.A. Martynov, K.V. Mitin, Phase equilibrium studies in the PbTe–Ga<sub>2</sub>Te<sub>3</sub> and PbTe–In<sub>2</sub>Te<sub>3</sub> systems for growing new nonlinear optical crystals of PbGa<sub>6</sub>Te<sub>10</sub> and PbIn<sub>6</sub>Te<sub>10</sub> with transparency extending into the far-IR, J. Alloys Compd. 612 (2014) 386–391.
- [59] A. Fiore, G. Morello, B.F. Scremin, Raman and photoluminescence spectra of ZnTe/ CdSe and ZnTe/CdTe tetrapod shaped nano-hetero structures, Superlattice. Microst. 113 (2018) 143–146.
- [60] C.-H. Lo, Master's Degree Thesis, Tamkang University, 2005.
- [61] C.-W. Chen, M.-H. Lee, Y.-T. Lin, Electro-optical modulation for a boron nitride nanotube probed by first-principles calculations, Appl. Phys. Lett. 89 (22) (2006): 223105.
- [62] R. He, Z.S. Lin, M.-H. Lee, C.T. Chen, Ab initio studies on the mechanism for linear and nonlinear optical effects in YAl<sub>3</sub>(BO<sub>3</sub>)<sub>4</sub>, J. Appl. Phys. 109 (10) (2011): 103510.
- [63] X. Jiang, L. Kang, S. Luo, P. Gong, M.-H. Lee, Z. Lin, Development of nonlinear optical materials promoted by density functional theory simulations, Int. Mod. Phys. B 28 (27) (2014): 1430018.
- [64] M. Sun, G. Wang, J. Yao, The Kurtz-Perry powder technique revisited: a study of the effect of reference selection on powder second-harmonic generation response, Molecules 28 (3) (2023) 1116–1165.
- [65] M. Sun, J. Yao, Ba<sub>2</sub>HgTe<sub>5</sub>: a Hg-based telluride with giant birefringence induced by linear [HgTe<sub>2</sub>] units, Inorg. Chem. Front. 9 (19) (2022) 5024–5031.
- [66] S.K. Kurtz, T.T. Perry, A powder technique for the evaluation of nonlinear optical materials, J. Appl. Phys. 39 (8) (1968) 3798–3813.
- [67] S.J. Clark, M.D. Segall, C.J. Pickard, P.J. Hasnip, M.I. Probert, K. Refson, M. C. Payne, First principles methods using CASTEP, Z. Krist-cryst. Mater. 220 (5–6) (2005) 567–570.
- [68] W. Kohn, L.J. Sham, Self-consistent equations including exchange and correlation effects, Phys. Rev. 140 (4A) (1965) A1133.
- [69] P. Hohenberg, W. Kohn, Inhomogeneous electron gas, Phys. Rev. 136 (3B) (1964) B864.
- [70] A.M. Rappe, K.M. Rabe, E. Kaxiras, J.D. Joannopoulos, Optimized pseudopotentials, Phys. Rev. B 41 (2) (1990) 1227–1230.
- [71] J.S. Lin, A. Qteish, M.C. Payne, V. Heine, Optimized and transferable nonlocal separable ab initio pseudopotentials, Phys. Rev. B 47 (8) (1993) 4174–4180.
- [72] M.-H. Lee, J.-S. Lin, M. Paynea, V. Heine, V. Milman, S. Crampin, Kinetic energy tuning for optimising pseudopotentials and projector reduction, Psi-k. Newsl. Highlight 67 (1994).
- [73] J. Lin, M.-H. Lee, Z.-P. Liu, C. Chen, C.J. Pickard, Mechanism for linear and nonlinear optical effects in  $\beta$ –BaB<sub>2</sub>O<sub>4</sub> crystals, Phys. Rev. B 60 (19) (1999): 13380.
- [74] V. Milman, K. Refson, S. Clark, C. Pickard, J. Yates, S.-P. Gao, P. Hasnip, M. Probert, A. Perlov, M. Segall, Electron and vibrational spectroscopies using DFT,

- plane waves and pseudopotentials: CASTEP implementation, J. Mol. Struc-Theochem 954 (1–3) (2010) 22–35.

  [75] K. Refson, P.R. Tulip, S.J. Clark, Variational density-functional perturbation theory for dielectrics and lattice dynamics, Phys. Rev. B 73 (15) (2006): 155114.
- [76] K. Miwa, Prediction of Raman spectra with ultrasoft pseudopotentials, Phys. Rev. B 84 (9) (2011): 094304.